THE JOURNAL OF PHYSICAL CHEMISTRY Letters

Letter

pubs.acs.org/JPCL

Photoinduced Reversible Structural Transformations in Free-Standing $CH_3NH_3PbI_3$ Perovskite Films

Ronen Gottesman,[†] Laxman Gouda,[†] Basanth S. Kalanoor, Eynav Haltzi, Shay Tirosh, Eli Rosh-Hodesh, Yaakov Tischler, and Arie Zaban*

Department of Chemistry, Center for Nanotechnology & Advanced Materials, Bar-Ilan University, Ramat Gan 52900, Israel

Claudio Quarti, Edoardo Mosconi, and Filippo De Angelis

Computational Laboratory for Hybrid/Organic Photovoltaics (CLHYO), CNR-ISTM, Via Elce di Sotto 8, I-06123 Perugia, Italy

Supporting Information

ABSTRACT: In the pursuit to better understand the mechanisms of perovskite solar cells we performed Raman and photoluminescence measurements of free-standing $CH_3NH_3PbI_3$ films, comparing dark with working conditions. The films, grown on a glass substrate and sealed by a thin glass coverslip, were measured subsequent to dark and white-light pretreatments. The extremely slow changes we observe in both the Raman and photoluminescence cannot be regarded as electronic processes, which are much faster. Thus, the most probable explanation is of slow photoinduced structural changes. The $CH_3NH_3PbI_3$ transformation between the dark and the light structures is reversible, with faster rates for the changes under illumination. The results seem to clarify several common observations associated with solar cell mechanisms, like performance improvement under light soaking. More important is the call for solar-cell-related investigation of $CH_3NH_3PbI_3$ to take the photoinduced structural changes into consideration when measuring and interpreting the results.

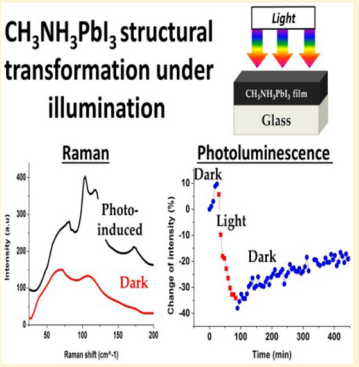

Photovoltaic solar cells based on methylammonium lead trihalide perovskite absorbers ($CH_3NH_3PbX_3$ or $MAPbX_3$, where X = Br, Cl, I) have reported certified efficiencies as high as 20.1%. Since the first reported perovskite-sensitized solar cell in a dye-sensitized solar cell (DSSC) configuration,[1] these absorbers were implemented in three other device architectures, all yielding more than 15% efficiency.[2−4] The structural diversity ranged from meso-superstructures[2] (replacing the nanoporous TiO_2[5] with an alumina scaffold) to mesoscopic[3] and planar junction[4] devices. The fact that the physics of each of these three devices is fundamentally different is an indication that $MAPbX_3$ materials are very unique.[6] The hybrid perovskites are ambipolar,[7−9] can efficiently transport both electrons and holes,[10,11] and possess unusually long electron and hole diffusion lengths.[12,13] Recently, $MAPbX_3$ perovskites have shown lasing capabilities,[14,15] been incorporated in bright light-emitting diodes,[16] and also used for photovoltachromic cells for building integration;[17] however, most of the fundamental questions concerning why these materials are so effective at generating and transporting photocurrents still remain unanswered. Despite the rapid increase in $MAPbX_3$ solar cell efficiency associated with device evolution,[18−20] optimization and full characterization of devices continues to be a major assignment for researchers. Advanced characterization of $MAPbX_3$ solar cells is already in progress;[21−23] however, structural and photophysical studies of isolated, stand-alone (i.e., no selective contacts) perovskite thin films under solar cell working conditions are still uncommon.

We report a study of free-standing films of $MAPbI_3$ that were deposited on glass, without any electrical contacts. We investigated the effect of light on these films and observed slow, gradual changes in the Raman spectra and in the photoluminescence (PL) intensity under illumination. The changes were reversible, moving between light and dark conditions, although the reverse process to the original dark values was much slower. The reversibility proved that the perovskite was not degraded during the measurement, which was also supported by steady-state absorption and XRD measurements. The changes were too slow to be interpreted by electronic processes, leaving only the option of slow and gradual photoinduced structural changes to the perovskite films.

The $MAPbI_3$ thin films were deposited on glass substrates using a sequential deposition method,[3] followed by sealing with a Surlyn resin and a 0.5 mm coverslip on top. (See the Experimental Methods for full details.) Throughout all experiments, the temperature was maintained at 25 °C (±1 °C). The illumination source was a white-light LED, which illuminated the entire sample and did not focus directly on the

Received: May 14, 2015
Accepted: June 5, 2015
Published: June 8, 2015

DOI: 10.1021/acs.jpclett.5b00994
J. Phys. Chem. Lett. 2015, 6, 2332−2338

measured area. The LED's spectrum was without any emission in the IR, which could heat up the films, and its intensity was <10 mW/cm^2 (0.1 sun). In both the Raman and the PL measurements, illumination by the measuring device (i.e., a laser for the Raman and a 400 nm band of a Xe lamp of the fluorometer) was significantly shorter than the low-intensity illumination by the LED. For each data point, the Raman laser and the monochromatic PL excitation were ON for 10 and 3 s, respectably, while illumination with the LED lasted from tens of minutes to a few hours. In all cases, the samples were not moved during a dark−light−dark cycle ensuring measurements of the same spot. Reproducibility of the results was validated by multiple dark−light−dark cycles on a single spot and by comparison of various spots on a single film or on different samples.

We used micro-Raman spectroscopy to characterize the $MAPbI_3$ structure before LED illumination (dark, hereafter) and upon LED illumination for varying durations. Raman spectroscopy is an optical mean of probing the vibrational modes of materials, which due to the specificity of these vibrational signatures, can provide detailed information about the composition, stoichiometry, degree of crystallinity, and crystalline phase of the materials in question. Confocal micro-Raman is a specially designed method for obtaining Raman spectra from specific locations within a sample, with the resolution and depth sectioning capability of a confocal microscope. When implemented in a confocal microscopic with suitable xyz-stages, Raman mapping of thin film samples can be performed in all three spatial dimensions. The confocal configuration can also provide information on the how the excitation and Raman scattering beams are propagating through and focusing in the sample. First, a laser of one specific wavelength is focused onto the sample using an objective lens and due to the vibrations intrinsic to the material, different colors of light are scattered, which indicate the frequency of the vibrations. The backscattered light is collected via the same objective and collimated, and the Rayleigh scattering peak is filtered using a high-performance Raman edge or notch filter. The cleaned Raman signal is then spatially filtered by focusing it through a confocal pinhole and finally sent into a high-resolution spectrometer. The final result is a spectrum that displays the intensity of the inelastically scattered light in wavenumbers relative to the wavelength of the exciting laser. An illustration of our optical setup is shown in Figure S1 in the Supporting Information (SI). In place of a physical pinhole, we obtain confocality by focusing the backscattered Raman signal onto the end of an optical fiber, which is then imaged onto the slit of the spectrometer.

In our micro-Raman measurements, the $MAPbI_3$ samples were excited using a 532 nm laser and a long working distance (4.5 mm), 100× objective with numerical aperture of 0.75. The longer working distance objective enabled easier side coupling of the LED sample illumination, as shown in Scheme 1. The LED was turned off during each Raman signal was taken in order to avoid any interference with the measurements and immediately turned back on again afterward. The optical fiber used to create the confocal pinhole had a 50 μm core diameter, and the two Raman filters were ion-beam-sputtered "razor-edge long pass filters" from Semrock. The laser excitation intensity was kept to a minimum (~16 KW/cm^2) so as not to burn the layers, and integration times were increased accordingly. We address later the importance of the laser's power to avoid degradation.

Scheme 1. Illustration of the Measurement System[a]

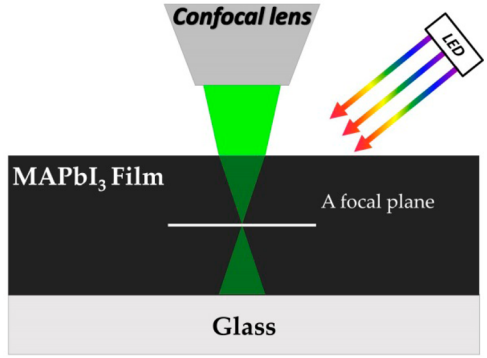

[a]Thin film of $MAPbI_3$, deposited on a glass substrate (the sealing coverslip is not shown here), is placed beneath the objective of the micro-Raman system (λ_{exc} = 532 nm). A white LED positioned a few centimeters away from the substrate was used for illumination.

In the following paragraphs we discuss the Raman spectra shape and peak designation. We wish to emphasize that the Raman signal of the $MAPbI_3$ is prone to slight variations when changing parameters such as (i) type of substrate (glass/FTO or a mesoporous metal-oxide film), (ii) deposition method (1-step method,[2] or a sequential deposition method[3]), and (iii) Raman measurement procedure (resonance or nonresonance conditions, the laser's energy, and optical setup such as specific types of filters used in the system). Consequently, we have compared qualitatively (see Table S1 in the SI) previous data with our own experimental Raman taken in the dark, shown in Figure 1A. We have concluded that both sets of data are in

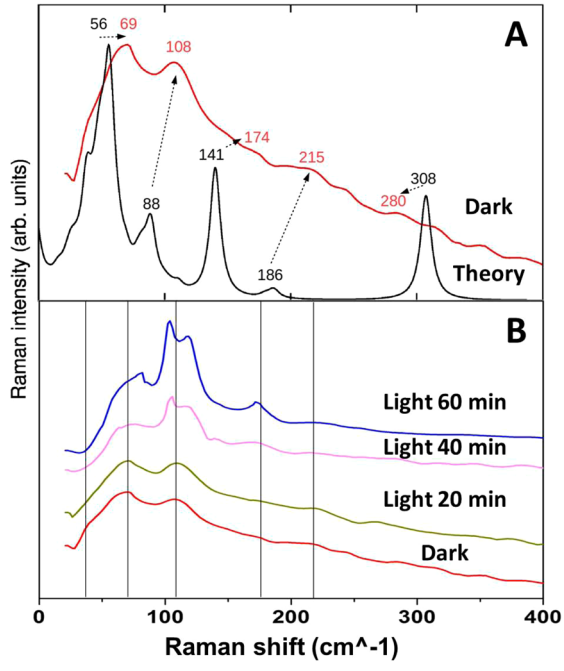

Figure 1. (A) Experimental (taken in the dark) and theoretical Raman spectra of a $MAPbI_3$ film, along with the main representative vibrational peaks. (B) Raman spectra of the same film taken in the dark and following illumination for 20, 40, and 60 min, showing photoinduced structural changes of the $MAPbI_3$. The cascade presentation of the four spectra and the thin vertical lines are set to improve visualization.

DOI: 10.1021/acs.jpclett.5b00994
J. Phys. Chem. Lett. 2015, 6, 2332−2338

overall agreement because they present many of the vibrational frequencies assigned to the $MAPbI_3$.[24−27] Two broad signals are present, one in the region between 50 and 70 cm^{-1} and the other between 105 and 120 cm^{-1}. The observed shifts of the Raman peaks (~10 cm^{-1}) are not completely unexpected and are discussed. In particular, the band at 108 cm^{-1} was reported at 119 cm^{-1} in our previous work, but such band was originally associated with the libration of the MA cations,[24] and thus its frequency is reasonably very sensitive to the local structure of the inorganic framework. For instance, Grancini et al. showed that this band shifts from at 119 to 108 cm^{-1}, going from a mesoporours to a planar $MAPbI_3$ sample.[26] This result is consistent with the finding of Choi et al., which highlighted a large degree of structural disorder for the inorganic framework mesoporous $MAPbI_3$ samples.[28] As a result, each organic MA cation is subjected to a different local environment that affects the vibrational frequencies, especially for the libration vibrations. Similar variations of the vibrational frequencies and relative intensities have also been found in other systems characterized by consistent disorder, as in graphene.[29] These arguments once more point out the fact that hybrid lead iodide perovskites resemble much more hybrid and organic systems, characterized by a large disorder, than their fully inorganic counterparts, for which the vibrational signals are generally very resolved.[30] In addition, they point out the necessity in future studies to define a shared procedure for the sample preparation synthesis and the measurement of the Raman spectrum of this class of materials.

The experimental band falling at 69 cm^{-1} can be assigned to the theoretical band (see Computational Methods in the SI) predicted around 56 cm^{-1}, consisting mainly in the bending of the I−Pb−I bonds and in the consequent liberation of the cations due to the deformation of the inorganic cage. Different vibrational frequencies for the Pb−I bending mode of $MAPbI_3$ have been proposed in the literature, between 52[25] and 71 cm^{-1}.[27] In previous works, a weak band at 94 cm^{-1} was found, assigned by DFT calculations to libration modes of the organic cations coupled to Pb−I stretching.[24] In the present Raman spectra, we did not observe such signal libration and Pb−I stretching mode that corresponds to the Raman signal calculated at 88 cm^{-1}. It is possible that this Raman signal is hidden below the more intense band at 108 cm^{-1}. On the contrary, the intense band at 108 cm^{-1} has no parallel in the theoretically calculated spectrum. Current DFT simulations agree with previous simulations that the vibrational features in the region of 100−200 cm^{-1} are associated with pure librations of the MA cations; however, on the theoretical side, the accurate prediction of the frequency and intensity of these vibrations is computationally complex. This is due to the fact that it should take into consideration anharmonic effects, together with the well-known rotational dynamics of the MA cations,[31] which are not accessible from out static picture. From the experimental side, the rotational dynamics of the organic counterpart also complicates the assignment of the vibrational features, in terms of specific vibrational eigenvectors or symmetry arguments. This is because the material, in particular, the organic component, has no fixed structure, but it explores different structural conformations during the time, as also shown by ab initio molecular dynamic simulations.[32] Similar problems in the peak assignment of IR and Raman spectra are quite common for all systems with a flexible structure, such as low-crystalline polymers[33] and biological systems.[34] We therefore limit ourselves to assign the features at 108 and at 174 cm^{-1} to the librations of the MA cations. In particular, the experimental signal at 174 cm^{-1} can be reasonably assigned to the signal calculated at 141 cm^{-1}. Current DFT simulations predict a rather intense band at ca. 308 cm^{-1}, associated with inner vibration of the molecule around the CN bond, that is, to the torsional vibration. The overestimation of the theoretical intensity of this transition is likely due to computational limitations inherent to our approach. Similar overestimations have been found before by the present authors[24] when a blue shift was observed and an intensity of the torsional vibration decreased, with an increase in the material order. In this sense, the presence of more bands at 280, 315, and 350 cm^{-1} in the region of the torsional vibration can be associated with the presence of material domains with a different degree of order.

Figure 1B presents four Raman spectra of the perovskite film, measured in the dark and following different periods of low-intensity (<0.1 sun) white-light (LED) illumination. Upon illumination we observe gradual spectral changes that represent transformation into a new photoinduced perovskite structure. When illumination is turned off the Raman spectrum slowly returns to the original dark shape, indicating retransformation of the photoinduced structure to the original one. While the light-induced structural transformation lasted tens of minutes, the backward process required several hours in the dark. These reversible, photoinduced spectral changes were measured with different samples and as successive cycles of the same perovskite film. Both the illumination intensity and the temperature affected the process rate, showing slower structural transformation at lower temperatures or light intensities. A typical cycle required small focus adjustments to follow the associated refractive index changes (unpublished results).

The PL measurements were performed in a Cary Eclipse fluorescence spectrophotometer in a steady-state mode. Similar sealed $MAPbI_3$ films deposited on glass were excited with 390 nm monochromatic light, generating a PL peak at 770 nm. The emission was probed in the wavelength range of 500−900 nm with a scan rate of 9600 nm/min. The sample was placed at 20° angle with respect to the detector, facing a LED similar to the one used in the Raman experiments for white-light illumination (Scheme 2). Here also, the LED was turned off during each PL scan to avoid any interference with the measurements.

The experimental cycle extending over a period of 11 to 12 h involved a PL measurement every 6 min. The cycles were divided into three sections: dark storage between measurements, constant LED illumination excluding the measurement time, and dark again. Figure 2 shows the variation of PL intensity during a typical cycle. The variations are presented in percentage relative to the first measurement point taken in the dark. The initial dark stage was 25 min, the LED illumination lasted 1 h, and for the remaining time the samples were kept in the dark.

Figure 2 shows a strong, accumulative effect of white light illumination on the PL intensity. Within 1 h of illumination (<0.1 sun) the PL gradually decreased by ~40%. Turning the LED off started a very slow recovery of the PL reaching 15% less than the original value after 10 h. Full recovery required 12−15 h. As shown in Figure S2 in the SI, the shape and position of the PL peak did not change during the 12 h cycle shown in Figure 2. The only varying parameter was the peak intensity. Here also, comparable results were obtained with several samples or by successive measurement cycles of the same sample following 24 h recovery in the dark.

DOI: 10.1021/acs.jpclett.5b00994
J. Phys. Chem. Lett. 2015, 6, 2332−2338

Scheme 2. Illustration of the PL Measurement System[a]

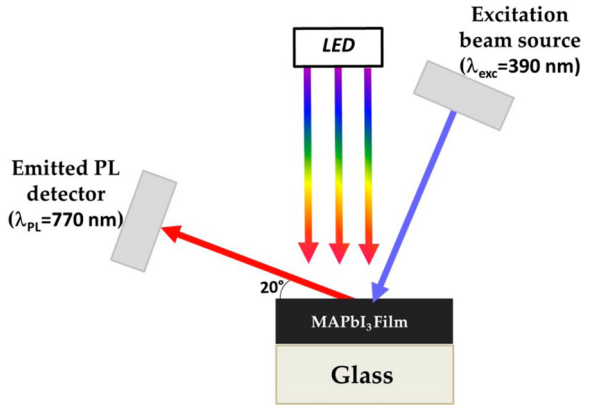

[a]Thin film of $MAPbI_3$, deposited on a glass substrate (the sealing coverslip is not shown here), is placed at a 20° with respect to the emission detector ($\lambda_{excitation}$ = 390 nm, $\lambda_{photoluminescence}$ = 770 nm). A white LED positioned a few centimeters away from the substrate was used for white-light illumination.

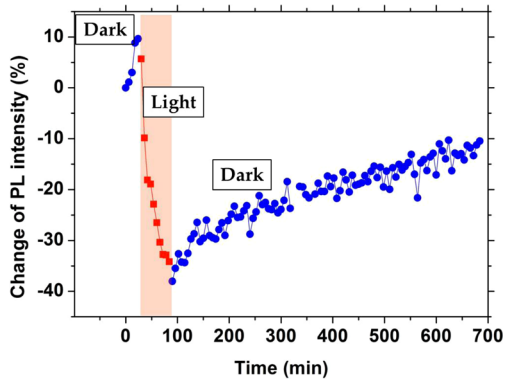

Figure 2. PL measurements performed in 6 min intervals throughout a dark–light–dark cycle, showing strong, accumulative effect of white-light illumination on the PL intensity. The period was divided into three stages: the initial dark (blue circles) stage lasted 25 min, then sample was illuminated (red squares) for 1 h, and in the remaining time of 12 h the samples were kept in the dark (again, blue circles).

Before we proceed into interpretation of the results, it is important to discuss the possibility of photoinduced degradation of the $MAPbI_3$ films. In other words, we need to show that our observations are not a result of gradual degradation of the perovskite under illumination. The highest concerns relate to the Raman measurements, where a laser is focused onto the film.

It is well known that $MAPbI_3$ perovskites can undergo rapid degradation under elevated temperatures and humidity,[35] although there are reports of stable systems under specific conditions.[36] A typical degradation process results in PbI_2 formation and color changes, both being a detectable property.[25,37−40] Consequently, we examined the films by UV–vis spectroscopy, optical microscopy, and XRD, finding no degradation in our samples during the dark–light–dark procedure. UV–vis absorption was measured by a procedure similar to that used for the PL, showing no spectral changes throughout the experimental cycle (Figure S3 in the SI). XRD measurements were also done along a dark–light–dark cycle using both a white LED and a 532 nm laser (<10 mW/cm^2, 0.1 sun). The results presented in Figure S4 in the SI demonstrate the stability of our $MAPbI_3$ samples under these conditions. The small PbI_2 peak, originating from PbI_2 residue of the sequential deposition method,[41] did not change its intensity the entire length of the measurement, as would be expected for $MAPbI_3$ decomposition.

However, the most convincing evidence of the stability of the $MAPbI_3$ films under the specific measurement conditions of this study is the full reversibility over many cycles. As previously mentioned, for both the Raman and the PL we conducted consecutive dark–light–dark cycles of a single spot within a film. The reproducibly of the variation between light and dark and the return to the original PL and Raman spectra at the end of each cycle leaves no room for $MAPbI_3$ degradation. We attribute this stability to two experimental factors: (i) The films were well-sealed in a dry glovebox, thus preventing any interaction with moisture throughout the experiments. Indeed, a reference sample that was not sealed exhibited degradation, noticeable by color change and permanent disappearance of the $MAPbI_3$ Raman features. (ii) The Raman laser power was adjusted to an optimal value that allows for the fastest collection of the spectra while not damaging the film. Practically the laser power was 16 KW/cm^2 (using a 500 μW laser), and the acquisition time of each spectrum lasted 10 s, averaging 10 consecutive 1 s spectra. When the illumination power or acquisition time increased by an order of magnitude, we noticed degradation even in sealed samples (by both optical and spectral means).

The photoinduced changes of both the Raman spectra and the PL intensity of the free-standing $MAPbI_3$ films can be characterized as being: reversible, slow for the forward process (tens of minutes), and very slow for the return to the original dark state (hours). Excluding electronic processes that are significantly faster and chemical degradation that is not observed, we believe that the only process that fits our results is photoinduced structural modification.

We offer two possible options for a structural modification under illumination: (i) rearrangement of the inorganic Pb–I scaffold to accommodate alignment or enhanced rotation of the MA cation and (ii) structural response to ion motion in the film.

As proposed in our recent study,[42] illumination that weakens the hydrogen bond between the MA cation and the inorganic scaffold enhances the rotational freedom of the MA cations. These dipole cations may align along an electric field, if present, or generate aligned domains by dipole–dipole interactions. The alignment should occur very fast, but the adjustment of the inorganic scaffold may be much slower, requiring long-time scales, as previously reported. In contrast with our previous study that involved photoconductivity to examine perovskite films under illumination, here we measured free-standing $MAPbI_3$ films with no applied biases. Consequently, it seems that dipole–dipole interactions or enhanced rotation of the MA cations are sufficient to derive structural changes the $MAPbI_3$ perovskite.

This understanding is supported by XRD measurements throughout the dark–light–dark cycle. As previously calculated,[43] structural transitions resulting from alignment of the MA dipoles in the inorganic scaffold should be reflected in the relative intensity of the peaks at 2θ values of 23.54 and 24.55°. The changing of the peaks ratio corresponds to a change in the rotation angle along the c axis of the octahedra. The experimental results measured over four cycles show reproducible and reversible variation of the 24.55/23.54° peak intensity

DOI: 10.1021/acs.jpclett.5b00994
J. Phys. Chem. Lett. 2015, 6, 2332−2338

ratio, moving from dark to light pretreatment (Figure S4 in the SI).

The second option attributes the observed Raman and PL variations to ions movement in the film. We examine this option due to the growing number of publications regarding ion movement in $MAPbX_3$ devices,[44−48] although, these are conceptually different from free-standing, contactless films. To investigate the possibility of ion movement in our $MAPbI_3$ films, we performed Rutherford backscattering (RBS) measurements in the dark−light−dark cycle.

RBS is a sensitive tool that generates atomic depth profiles in thin films via modeling of the measured spectra. It is a widely used technique based on the approximation of the coulomb interaction of point charges for analyzing the near-surface region of solids.[49] A sample is bombarded with ions at an energy in the MeV range (typically 0.5−4 MeV), and the energy of the backscattered ions is recorded with an energy sensitive detector, typically a solid-state detector. The method allows quantitative composition determination of a material and depth profiling of individual elements. There is no need for reference samples, and the depth resolution can be on the order of several nanometers with high sensitivity for heavy elements. Consequently, it provides quantitative information on atomic motion along the beam axis between two successive measurements.[50−52] Here we used unsealed $MAPbI_3$ films that were placed in the vacuum chamber and a LED similar to that used in the Raman and PL experiments for the illumination. The measurements were performed in a "raster scan" mode to minimize the interaction time of the ion beam with the sample. We have learned that long measurement over a single spot can damage the $MAPbI_3$, as often seen in RBS measurements of "soft" organic samples.[53,54] Full experimental details and the measured spectra (Figure S5) are provided in the SI. Comparing the RBS spectra measured before and following white-light illumination display no energetic shift in the positions of the elemental edges of both Pb and I (the constituent elements of the perovskite film). In the case of ion movement, we would expect to see one of two effects: (i) the low-energy edges of the Pb and I peaks will broaden, indicating a penetration of the perovskite into the adjacent layer, or (ii) the Pb:I ratio will change if one of those ions diffuses from the perovskite layer. Consequently, without a need to model the spectra, we conclude that there is no ion movement in our free-standing $MAPbI_3$ films due to illumination. We are therefore left with the first explanation for the source of structural modification of $MAPbI_3$ under illumination: rearrangement of the inorganic Pb−I scaffold to accommodate alignment or enhanced rotation of the MA cations.

In conclusion, our results show that $MAPbI_3$ undergoes structural modification under illumination, which presumably affects its operation in a solar cell. On the basis of this understanding we would like to emphasize the following messages: (a) It should be taken into consideration that the crystal structure of $MAPbI_3$ under working conditions differs from that of dark conditions. (b) Performing measurements that involve $MAPbI_3$ illumination, one should consider light soaking prior to the actual measurement, if the structure at operation conditions is of interest. In the perspective of solar cells, it is probably safe to consider results when reaching the highest value of maximum power point (MPP), the point where the crystal structure transformation is finalized. (c) In the case of free-standing $MAPbI_3$ films the photoinduced structural changes seem to solely arise from rearrangement of the inorganic scaffold to accommodate alignment or enhanced rotation of the MA cations. This does not eliminate the possibility of ion movement in $MAPbI_3$-based devices, where selective contact and electrical fields might play another crucial role.

The structural changes can possibly explain the well-known hysteresis in $MAPbI_3$ solar cells as previously suggested by us and others.[36,42,55,56] Moreover, decay of exited electrons back into the ground state requires interaction with the rotating dipoles, which presumably affects the reorganization energy and thus the recombination rate. Finally, it is also possible that the free rotating dipoles are involved in charge screening, which can reduce recombination, a speculation that is currently under investigation. Although out of the scope of this paper, we want to raise the hypothesis that the photoinduced structure is more ordered than the dark structure. Currently this assessment is solely based on the fact that the Raman spectra of the illuminated samples exhibit much sharper and pronounced peaks.

EXPERIMENTAL METHODS

For the preparation of the perovskite film, we used PbI_2 and CH_3NH_3I as precursors. The CH_3NH_3I was synthesized using a procedure described elsewhere,[42] while commercial PbI_2 (99.99%, Sigma-Aldrich) was used without further purification. The entire synthesis was performed inside a glovebox. The substrates were 25 × 25 mm microscopic glass slides cleaned using plasma etching. For the lead iodide precursor, 1 M solution of PbI_2 in dimethyl sulfoxide (DMSO) was prepared and stirred overnight at 80 °C. The solution was filtered prior to use with a PTFE filter with a pore diameter of 0.45 μm. For the CH_3NH_3I precursor, a solution with a concentration of 32 mg/mL in 2-propanol was prepared right before the synthesis and kept at 60 °C. First, a film of PbI_2 was formed on the substrate after spin coating 100 μL of the PbI_2 solution at 4000 rpm for 60 s, followed by annealing at 100 °C for 60 min. Next, the annealed substrate was dipped in the CH_3NH_3I solution for 5 min. Immediately after the dipping, a dark-brown color was apparent, indicating the formation of the $CH_3NH_3PbI_3$ perovskite. After dipping in the CH_3NH_3I solution the substrate coated with the perovskite layer was washed with clean 2-propanol. Finally, the film was annealed at 100 °C for 45 min. Before the measurements, each substrate was sealed with a Surlyn film as a spacer and a 0.1 mm thick glass cover slide using fast annealing for 2 min at 100 °C to melt the Surlyn tape.

ASSOCIATED CONTENT

Supporting Information

Raman, computational details, and RBS measurements, illustrations of the experimental optical setup, XRD data, absorption, and additional PL data are presented. The Supporting Information is available free of charge on the ACS Publications website at DOI: 10.1021/acs.jpclett.5b00994.

AUTHOR INFORMATION

Corresponding Author

*E-mail: zabana@mail.biu.ac.il.

Author Contributions

†R.G and L.G contributed equally to this work.

Notes

The authors declare no competing financial interest.

DOI: 10.1021/acs.jpclett.5b00994
J. Phys. Chem. Lett. 2015, 6, 2332−2338

■ ACKNOWLEDGMENTS

We thank Dr. Olga Girshevitz and Dr. Vladimir Richter for their valuable assistance and performing the RBS measurements. We also acknowledge the Israel Strategic Alternative Energy Foundation (I-SAEF) and the "Tashtiyot" Program of the Israeli Ministry of Science & Technology for funding this research. Fellowship for L.G. from the European Union Seventh Framework Program Destiny Project under grant 316494 is acknowledged.

■ REFERENCES

(1) Kojima, A.; Teshima, K.; Shirai, Y.; Miyasaka, T. Organometal Halide Perovskites as Visible-Light Sensitizers for Photovoltaic Cells. *J. Am. Chem. Soc.* **2009**, *131*, 6050−6051.
(2) Lee, M. M.; Teuscher, J.; Miyasaka, T.; Murakami, T. N.; Snaith, H. J. Efficient Hybrid Solar Cells Based on Meso-Superstructured Organometal Halide Perovskites. *Science* **2012**, *338*, 643−647.
(3) Burschka, J.; Pellet, N.; Moon, S.-J.; Humphry-Baker, R.; Gao, P.; Nazeeruddin, M. K.; Gratzel, M. Sequential Deposition as a Route to High-Performance Perovskite-Sensitized Solar Cells. *Nature* **2013**, *499*, 3−7.
(4) Liu, M.; Johnston, M. B.; Snaith, H. J. Efficient Planar Heterojunction Perovskite Solar Cells by Vapour Deposition. *Nature* **2013**, *501*, 395−398.
(5) Gottesman, R.; Tirosh, S.; Barad, H.-N.; Zaban, A. Direct Imaging of the Recombination/Reduction Sites in Porous TiO_2 Electrodes. *J. Phys. Chem. Lett.* **2013**, *4*, 2822−2828.
(6) Snaith, H. J. Perovskites: The Emergence of a New Era for Low-Cost, High-Efficiency Solar Cells. *J. Phys. Chem. Lett.* **2013**, *4*, 3623−3630.
(7) Giorgi, G.; Fujisawa, J.-I.; Segawa, H.; Yamashita, K. Small Photocarrier Effective Masses Featuring Ambipolar Transport in Methylammonium Lead Iodide Perovskite: A Density Functional Analysis. *J. Phys. Chem. Lett.* **2013**, *4*, 4213−4216.
(8) Bisquert, J. Nano-Enabled Photovoltaics. Progress in Materials and Methodologies. *J. Phys. Chem. Lett.* **2013**, *4*, 1051−1052.
(9) Heo, J. H.; Im, S. H.; Noh, J. H.; Mandal, T. N.; Lim, C.-S.; Chang, J. A.; Lee, Y. H.; Kim, H. J.; Sarkar, A.; Nazeeruddin, M. K. Efficient Inorganic−organic Hybrid Heterojunction Solar Cells Containing Perovskite Compound and Polymeric Hole Conductors. *Nat. Photonics* **2013**, *7*, 486−491.
(10) Laban, W. A.; Etgar, L. Depleted Hole Conductor-Free Lead Halide Iodide Heterojunction Solar Cell. *Energy Environ. Sci.* **2013**, *6*, 3249−3253.
(11) Etgar, L.; Gao, P.; Xue, Z.; Peng, P.; Chandiran, A. K.; Liu, B.; Nazeeruddin, M. K.; Gratzel, M. Mesoscopic $CH_3NH_3PbI_3/TiO_2$ Heterojunction Solar Cells. *J. Am. Chem. Soc.* **2012**, *134*, 17396−17399.
(12) Xing, G.; Mathews, N.; Sun, S.; Lim, S. S.; Lam, Y. M.; Gratzel, M.; Mhaisalkar, S.; Sum, T. C. Long-Range Balanced Electron- and Hole-Transport Lengths in Organic-Inorganic $CH_3NH_3PbI_3$. *Science* **2013**, *342*, 344−347.
(13) Stranks, S. D.; Eperon, G. E.; Grancini, G.; Menelaou, C.; Alcocer, M. J. P.; Leijtens, T.; Herz, L. M.; Petrozza, A.; Snaith, H. J. Electron-Hole Diffusion Lengths Exceeding 1 Micrometer in an Organometal Trihalide Perovskite Absorber. *Science* **2013**, *342*, 341−344.
(14) Deschler, F.; Price, M.; Pathak, S.; Klintberg, L. E.; Jarausch, D. E.; Higler, R.; Huettner, S.; Leijtens, T.; Stranks, S. D.; Snaith, H. J. High Photoluminescence Efficiency and Optically-Pumped Lasing in Solution-Processed Mixed Halide Perovskite Semiconductors. *J. Phys. Chem. Lett.* **2014**, *5*, 1421−1426.
(15) Sutherland, B. R.; Hoogland, S.; Adachi, M. M.; Wong, C. T. O.; Sargent, E. H. Conformal Organohalide Perovskites Enable Lasing on Spherical Resonators. *ACS Nano* **2014**, *8*, 10947−10952.
(16) Tan, Z.-K.; Moghaddam, R. S.; Lai, M. L.; Docampo, P.; Higler, R.; Deschler, F.; Price, M.; Sadhanala, A.; Pazos, L. M.; Credgington, D. Bright Light-Emitting Diodes Based on Organometal Halide Perovskite. *Nat. Nanotechnol.* **2014**, *9*, 1−6.
(17) Cannavale, A.; E Eperon, G.; Cossari, P.; Abate, A.; Snaith, H.; Gigli, G. Perovskite Photovoltachromic Cells for Building Integration. *Energy Environ. Sci.* **2015**, *8*, 1578−1584.
(18) Park, N.-G. Organometal Perovskite Light Absorbers Toward a 20% Efficiency Low-Cost Solid-State Mesoscopic Solar Cell. *J. Phys. Chem. Lett.* **2013**, *4*, 2423−2429.
(19) Jeon, N. J.; Noh, J. H.; Kim, Y. C.; Yang, W. S.; Ryu, S.; Seok, S. Il. Solvent Engineering for High-Performance Inorganic−organic Hybrid Perovskite Solar Cells. *Nat. Mater.* **2014**, *13*, 1−7.
(20) Jeon, N. J.; Noh, J. H.; Yang, W. S.; Kim, Y. C.; Ryu, S.; Seo, J.; Seok, S. Il. Compositional Engineering of Perovskite Materials for High-Performance Solar Cells. *Nature* **2015**, *517*, 476−480.
(21) Stamplecoskie, K. G.; Manser, J. S.; Kamat, P. V. Dual Nature of the Excited State in Organic-Inorganic Lead Halide Perovskites. *Energy Environ. Sci.* **2015**, *8*, 208−215.
(22) Tidhar, Y.; Edri, E.; Weissman, H.; Zohar, D.; Hodes, G. Crystallization of Methyl Ammonium Lead Halide Perovskites: Implications for Photovoltaic Applications. *J. Am. Chem. Soc.* **2014**, *136*, 13249−13256.
(23) Bertoluzzi, L.; Sanchez, R. S.; Liu, L.; Lee, J.-W.; Mas-Marza, E.; Han, H.; Park, N.-G.; Mora-Sero, I.; Bisquert, J. Cooperative Kinetics of Depolarization in $CH_3NH_3PbI_3$ Perovskite Solar Cells. *Energy Environ. Sci.* **2015**, *8*, 910−915.
(24) Quarti, C.; Grancini, G.; Mosconi, E.; Bruno, P.; Ball, J. M.; Lee, M. M.; Snaith, H. J.; Petrozza, A.; Angelis, F. De. The Raman Spectrum of the $CH_3NH_3PbI_3$ Hybrid Perovskite: Interplay of Theory and Experiment. *J. Phys. Chem. Lett.* **2014**, *5*, 279−284.
(25) Ledinsky, M.; Löper, P.; Niesen, B.; Holovsky, J.; Yum, J.; De Wolf, S.; Fejfar, A.; Ballif, C. Raman Spectroscopy of Organic-Inorganic Halide Perovskites. *J. Phys. Chem. Lett.* **2015**, *6*, 401−406.
(26) Grancini, G.; Marras, S.; Prato, M.; Giannini, C.; Quarti, C.; De Angelis, F.; De Bastiani, M.; Eperon, G. E.; Snaith, H. J.; Manna, L.; et al. The Impact of the Crystallization Processes on the Structural and Optical Properties of Hybrid Perovskite Films for Photovoltaics. *J. Phys. Chem. Lett.* **2014**, *5*, 3836−3842.
(27) Park, B.; Jain, S. M.; Zhang, X.; Hagfeldt, A.; Boschloo, G.; Edvinsson, T. Resonance Raman and Excitation Energy Dependent Charge Transfer Mechanism in Halide-Substituted Hybrid Perovskite Solar Cells. *ACS Nano* **2015**, *9*, 2088−2101.
(28) Choi, J. J.; Yang, X.; Norman, Z. M.; Billinge, S. J. L.; Owen, J. S. Structure of Methylammonium Lead Iodide within Mesoporous Titanium Dioxide: Active Material in High-Performance Perovskite Solar Cells. *Nano Lett.* **2014**, *14*, 127−133.
(29) Ferrari, A. C. Raman Spectroscopy of Graphene and Graphite: Disorder, Electron-Phonon Coupling, Doping and Nonadiabatic Effects. *Solid State Commun.* **2007**, *143*, 47−57.
(30) Mihut, L.; Lefrant, S.; Baltog, I. Identification of the Symmetry of Phonon Modes in $CsPbCl_3$ in Phase IV by Raman and Resonance-Raman Scattering. *J. Appl. Phys.* **1997**, *82*, 5391−5395.
(31) Poglitsch, A.; Weber, D. Dynamic Disorder in Methylammoniumtrihalogenoplumbates (II) Observed by Millimeter-Wave Spectroscopy. *J. Chem. Phys.* **1987**, *87*, 6373−6378.
(32) Quarti, C.; Mosconi, E.; De Angelis, F. Structural and Electronic Properties of Organo-Halide Hybrid Perovskites from Ab Initio Molecular Dynamics. *Phys. Chem. Chem. Phys.* **2015**, *17*, 9394−9409.
(33) Quarti, C.; Milani, A.; Castiglioni, C. Ab Initio Calculation of the IR Spectrum of PTFE: Helical Symmetry and Defects. *J. Phys. Chem. B* **2013**, *117*, 706−718.
(34) Siebert, F.; Hildebrandt, P. *Vibrational Spectroscopy in Life Science*; Wiley-VCH Verlag: Berlin, 2008.
(35) Niu, G.; Guo, X.; Wang, L. Review of Recent Progress in Chemical Stability of Perovskite Solar Cells. *J. Mater. Chem. A* **2015**, *3*, 8970−8980.
(36) Hoke, E. T.; Slotcavage, D. J.; Dohner, E. R.; Bowring, A. R.; Karunadasa, H. I.; McGehee, M. D. Reversible Photo-Induced Trap Formation in Mixed-Halide Hybrid Perovskites for Photovoltaics. *Chem. Sci.* **2015**, *6*, 613−617.

DOI: 10.1021/acs.jpclett.5b00994
J. Phys. Chem. Lett. 2015, 6, 2332−2338

(37) Christians, J. a; Alexander, M. H. P.; Kamat, P. V. Transformation of the Excited State and Photovoltaic Efficiency of $CH_3NH_3PbI_3$ Perovskite upon Controlled Exposure to Humidified Air. *J. Am. Chem. Soc.* **2015**, *4*, 1530−1538.
(38) Misra, R. K.; Sigalit, A.; Baili, L.; Dmitri, M.; Iris, V.-F.; Lioz, E.; Eugene, A. K. Temperature- and Component-Dependent Degradation of Perovskite Photovoltaic Materials under Concentrated Sunlight. *J. Phys. Chem. Lett.* **2014**, *6*, 326−330.
(39) Jinli, Y.; Braden, D. S.; Dianyi, L.; Timothy, L. K. An Investigation of $CH_3NH_3PbI_3$ Degradation Rates and Mechanisms in Controlled Humidity Environments Using in Situ Techniques. *ACS Nano* **2015**, *9*, 1955−1963.
(40) Leguy, A.; Hu, Y.; Campoy-Quiles, M.; Alonso, M. I.; Weber, O. J.; Azarhoosh, P.; van Schilfgaarde, M.; Weller, M. T.; Bein, T.; Nelson, J. Reversible Hydration of $CH_3NH_3PbI_3$ in Films, Single Crystals, and Solar Cells. *Chem. Mater.* **2015**, *27*, 3397−3407.
(41) Wu, Y.; Islam, A.; Yang, X.; Qin, C.; Liu, J.; Zhang, K.; Penga, W.; Han, L. Retarding the Crystallization of PbI_2 for Highly Reproducible Planar-Structured Perovskite Solar Cells via Sequential Deposition. *Energy Environ. Sci.* **2014**, *7*, 2934−2938.
(42) Gottesman, R.; Haltzi, E.; Gouda, L.; Tirosh, S.; Bouhadana, Y.; Mosconi, E.; De Angelis, F.; Zaban, A. Extremely Slow Photoconductivity Response of $CH_3NH_3PbI_3$ Perovskites Suggesting Structural Changes under Working Conditions. *J. Phys. Chem. Lett.* **2014**, *5*, 2662−2669.
(43) Quarti, C.; Mosconi, E.; Angelis, F. De. Interplay of Orientational Order and Electronic Structure in Methylammonium Lead Iodide: Implications for Solar Cell Operation. *Chem. Mater.* **2014**, *26*, 6557−6569.
(44) Xiao, Z.; Yuan, Y.; Shao, Y.; Wang, Q.; Dong, Q.; Bi, C.; Sharma, P.; Alexei, G.; Jinsong, H. Giant Switchable Photovoltaic Effect in Organometal Trihalide Perovskite Devices. *Nature* **2015**, *14*, 193−198.
(45) Zhao, Y.; Liang, C.; Zhang, H. M.; Li, D.; Tian, D.; Li, G.; Jing, X.; Zhang, W.; Xiao, W.; Liu, Q.; et al. Anomalously Large Interface Charge in Polarity-Switchable Photovoltaic Devices: An Indication of Mobile Ions in Organic-Inorganic Halide Perovskites. *Energy Environ. Sci.* **2015**, *8*, 1256−1260.
(46) Almora, O.; Zarazua, I.; Mas-Marza, E.; Mora-Sero, I.; Bisquert, J.; Garcia-Belmonte, G. Capacitive Dark Currents, Hysteresis, and Electrode Polarization in Lead Halide Perovskite Solar Cells. *J. Phys. Chem. Lett.* **2015**, *6*, 1645−1652.
(47) Tress, W.; Marinova, N.; Moehl, T.; Zakeeruddin, S. M.; Nazeeruddin, M. K.; Grätzel, M. Understanding the Rate-Dependent J−V Hysteresis, Slow Time Component, and Aging in $CH_3NH_3PbI_3$ Perovskite Solar Cells: The Role of a Compensated Electric Field. *Energy Environ. Sci.* **2015**, *8*, 995−1004.
(48) Beilsten-Edmands, J.; Eperon, G. E.; Johnson, R. D.; Snaith, H. J.; Radaelli, P. G. Non-Ferroelectric Nature of the Conductance Hysteresis in $CH_3NH_3PbI_3$ Perovskite-Based Photovoltaic Devices. *Appl. Phys. Lett.* **2015**, *106*, 173502.
(49) Chu, W.-K.; Mayer, J. W.; Nicolet, M.-A. *Backscatering Spectroscopy*; Academic Press: New York, 1978.
(50) Jeynes, C.; Barradas, N. P.; Marriott, P. K.; Boudreault, G.; Jenkin, M.; Wendler, E.; Webb, R. P. Elemental Thin Film Depth Profiles by Ion Beam Analysis Using Simulated Annealing - a New Tool. *J. Phys. D: Appl. Phys.* **2003**, *97*, R97−R126.
(51) Cherniak, D. J.; Watson, E. B. Pb Diffusion in Zircon. *Chem. Geol.* **2000**, *139*, 198−207.
(52) Cherniak, D. .; Lanford, W.; Ryerson, F. Lead Diffusion in Apatite and Zircon Using Ion Implantation and Rutherford Backscattering Techniques. *Geochim. Cosmochim. Acta* **1991**, *55*, 1663−1673.
(53) Marée, C. H. M.; Kleinpenning, A.; Vredenberg, A. M.; Habraken, F. H. P. M. Ion Beam Analysis of Electropolymerized Porphyrin Layers. *Nucl. Instrum. Methods Phys. Res., Sect. B* **1996**, *118*, 301−306.
(54) Venkatesan, T.; Forrest, S. R.; Kaplan, M. L.; Murray, C. a.; Schmidt, P. H.; Wilkens, B. J. Ion-Beam-Induced Conductivity in Polymer Films. *J. Appl. Phys.* **1983**, *54*, 3150−3153.
(55) Snaith, H. J.; Abate, A.; Ball, J. M.; Eperon, G. E.; Leijtens, T.; Noel, N. K.; Stranks, S. D.; Wang, J. T.-W.; Wojciechowski, K.; Zhang, W. Anomalous Hysteresis in Perovskite Solar Cells. *J. Phys. Chem. Lett.* **2014**, *5*, 1511−1515.
(56) Chen, H.; Sakai, N.; Ikegami, M.; Miyasaka, T. Emergence of Hysteresis and Transient Ferroelectric Response in Organo-Lead Halide Perovskite Solar Cells. *J. Phys. Chem. Lett.* **2015**, *6*, 164−169.

DOI: 10.1021/acs.jpclett.5b00994
J. Phys. Chem. Lett. 2015, 6, 2332−2338